CHAPTER 11 Tropical atmosphere–ocean interactions

11.1 Introduction

The oceans cover about two thirds of the Earth's surface. Their average depth is about 4 km. Water is heavy stuff; the mass of 1 m^3 of water is 10^3 kg. The mass of the oceans is about 2×10^{14} kg. The mass of the atmosphere is about 250 times less, roughly 0.8×10^{12} kg. Not only is water dense, it has a very high heat capacity: about 4200 J kg^{-1} K^{-1}. In contrast, the heat capacity of air (at constant pressure) is only about 1000 J kg^{-1} K^{-1}. The total heat capacity of the oceans is thus about 1000 times larger than the total heat capacity of the atmosphere. When the oceans say "Jump," the atmosphere says "How high?"

The density of the atmosphere is highly variable, especially with height. In contrast, the density of sea water varies by only a few percent throughout the entire ocean; it is a complex but fairly weak function of temperature, salinity, and pressure. Because of the near-incompressibility of water, pressure effects (called "thermobaric" effects) are relatively unimportant; variations of the density are mainly due to changes in temperature and salinity. Warmer and fresher water is less dense and tends to float on top; colder and saltier water is more dense and tends to sink. Surface cooling and evaporation create dense water; surface heating and precipitation create light water. Note that the properties of the water are altered mainly near the surface; below the top hundred meters or so, the properties of water parcels remain nearly invariant, even over decades or centuries.

The ocean currents are typically very slow (centimeters per second) compared to the usual near-surface wind speeds, so for practical purposes the oceans can be considered to be at rest when air-sea momentum exchanges are considered. The property of the oceans that most directly affects the atmosphere is the sea surface temperature, which affects the upward longwave radiation, the sensible heat flux, and the latent heat flux. The roughness of the sea surface can also affect the efficiency of near-surface turbulent exchange. The albedo of the ocean is determined in part by the turbidity of the near-surface water, and of course by sea ice, where present. Sea ice also affects the sensible and latent heat fluxes, by presenting to the air a surface which can be much colder than the sea water below; and it can affect the atmospheric turbulence through its roughness and the presence of leads and other breaks in the ice.

Many properties of the atmospheric column can affect the ocean. These include the near-surface temperature, which influences sensible heat exchange and downward long wave radiation; the near-surface humidity which influences latent heat exchange and downward longwave radiation;, and cloudiness, which can affect the surface solar and terrestrial radiation. Precipitation also affects the salinity of the surface waters.

When the wind stress acts on the ocean, the Coriolis acceleration acts to turn the wind-induced surface current so that it does not have same direction as the surface stress. In the Northern Hemisphere, the Coriolis acceleration causes the surface current to move to the right of the surface wind, while in the Southern Hemisphere it moves to the left.

The ocean circulation is primarily wind-driven, but it does have an important buoyancy-driven component, called the thermohaline circulation.

The prevailing westerlies in middle latitudes induce a equatorward drift superimposed on a general eastward current in the upper ocean, and the prevailing easterlies in the tropics tend to cancel this equatorward drift out, while driving the surface currents back towards the west. The circulation of the upper oceans thus takes the form of a pair of huge "gyres," one in either hemisphere. The poleward currents, such as the Gulf Stream and Kuroshio, tend to be warmer than average at a given latitude, and the equatorward currents, such as the California Current and the Humboldt Current, tend to be cooler than average at a given latitude.

As already mentioned, the tradewinds induce a westward current in the upper ocean, thus tending to pile up warm water on the western side of each basin. There is a highly concentrated west-to-east return flow very close to the Equator and slightly below the surface, called the Equatorial Undercurrent.

11.2 The Walker Circulation

The Walker Circulation (named by Bjerknes, 1966) is an east-west overturning of the atmosphere above the tropical Pacific Ocean, with rising motion on the west side, over the so-called "Warm Pool," and sinking motion on the east side. The Walker Circulation can be viewed as a thermally excited stationary eddy. Although Walker Circulation is driven by the east-to-west sea surface temperature gradient, it also helps to maintain that gradient through mechanisms to be discussed later. For this reason, the Walker Circulation is best understood as a coupled ocean-atmosphere phenomenon. It undergoes strong interannual variability. Fig. 11.1 is a schematic illustration of the walker circulation and its relation to the surface wind field in the southern Hemisphere. The equatorward flow just west of South America can be viewed as the inflow to the ITCZ (which is generally north of the Equator in this region), and so it is in a sense a portion of the lower branch of the Hadley circulation. Fig. 11.2 shows the observed longitude-height cross sections of the zonal wind and vertical velocity, for January.

The Hadley Circulation is defined in terms of zonal averages, and so a particle participating in the Hadley Circulation through motions in the latitude-height plane cannot "escape" by moving to a different longitude. In contrast, the Walker Circulation is restricted to a narrow band of tropical latitudes, so that a particle participating in the Walker Circulation *can* escape by moving off to a different latitude; in fact, such meridional escapes are to be expected in view of the strong meridional motions associated with the Hadley Circulation. For this reason, we should not think of the Walker Circulation as a closed "race track;" it is better to view the Hadley and Walker Circulations as closely linked. For instance, a parcel may travel westward across the tropical Pacific in the lower branch of the Walker Circulation, ascend to the tropopause over the Warm Pool, and then move both poleward and eastward away from the Warm Pool, possibly descending in the subtropical eastern Pacific. It can then join the trades, and repeat its westward journey in the boundary layer.

An early description of the Walker circulation is given by Troup (1965), who described a toroidal circulation spanning the equatorial Pacific ocean. Troup presented data in which the mean 500-300 mb geopotential thickness for 120-140˚ E was 20 m greater than

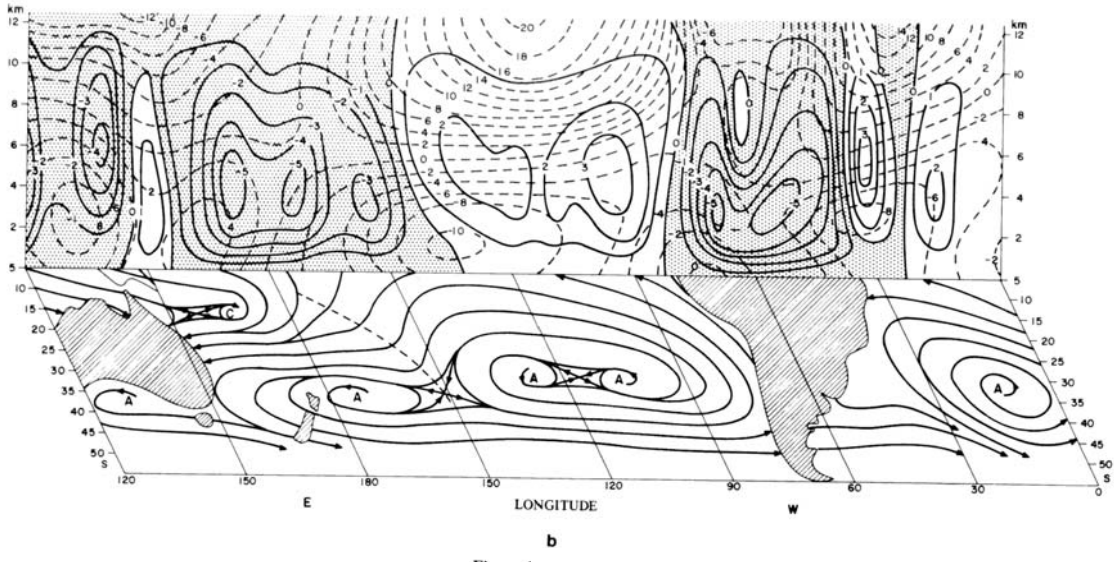

Figure 11.1: The Walker and Hadley Circulations. From Philander (1990).

that for 80-100˚ W. By the thermal wind equation (e.g. Holton 1992), this east-west thickness difference implies that the meridional geostrophic wind must decrease with height. Because the vertical gradient of meridional geostrophic wind is related to the zonal temperature gradient by the thermal wind relation, it can be shown that the zonal temperature gradient drives an ascending ageostrophic flow from the warm region to cold region. As Troup noted, the resulting distribution of ageostrophic motions is complicated, because it depends on the varying temperature differences and vertical motions across the different regions of the circulation. Troup found that westerly flow between 500 and 200 mb originates over the Indonesian region and terminates over the central and eastern equatorial Pacific; this upper-level flow is balanced by an easterly return flow, which he described as frictional ageostrophic flow down the pressure gradient. He noted that descent occurs over the central and eastern Pacific, while ascent occurs over the western Pacific and Indonesia.

Bjerknes (1969) theorized that when the equatorial cold tongue is well developed, the cool, dry air just above the surface cannot ascend to join the Hadley circulation. Instead, it is heated and moistened as it moves westward until it finally undergoes large-scale moist-adiabatic ascent over the Warm Pool. If there were no mass exchange with adjacent latitudes, a simple circulation would develop in which the flow is easterly at low levels and westerly at upper levels. Furthermore, the ascending motion in the west would adjust so as to cover a smaller surface area than the descending motion, which develops as a result of the balance between subsidence warming and radiative cooling. Mass continuity demands that the region of intense rising motion must occupy a smaller area than the region of weak sinking motion. When meridional mass exchange is considered, this simple picture has to be altered, because absolute angular momentum is exported to adjacent latitudes. Under steady-state conditions, the flux divergence of angular momentum at the equator must be balanced by an easterly surface wind stress. Thus surface easterlies on the equator are stronger than those imposed by the Walker circulation. The net result is that a thermally driven Walker cell is imposed on a background of easterly flow, the intensity of which depends on the strength of the angular momentum flux divergence. Apparently, Bjerknes was unaware of the paper by Troup (1965),

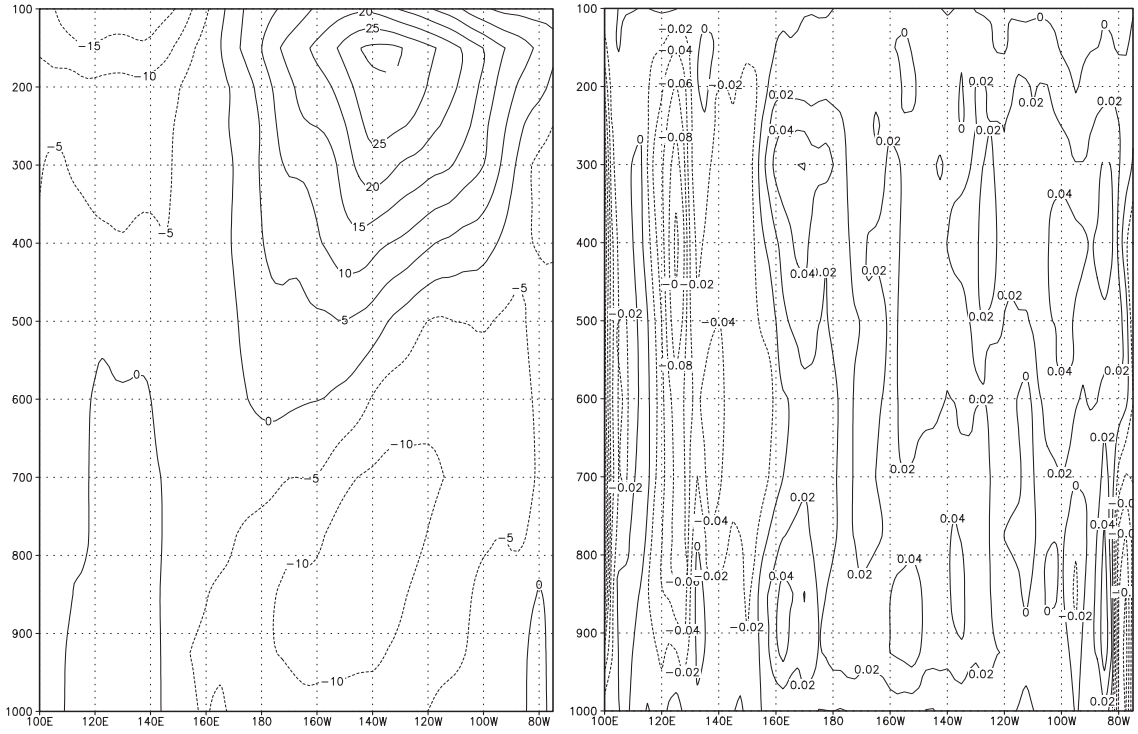

Figure 11.2: The longitude–height cross-sections of the zonal wind (left, in m s^{-1}) and vertical velocity (right, in Pa s^{-1}) along the Equator, for January, as analyzed by ECMWF.

as no reference was made to the earlier study.

Fig. 11.3 presents scaled *u*-ω wind vectors in the equatorial *x*-*z* plane for January 1989 from the ECMWF reanalysis dataset. We define *u* and ω as the zonal and vertical components of velocity in pressure coordinates. The vertical velocity was scaled by -300 m Pa^{-1} in order to account for the much smaller speed of the vertical motions as compared with the horizontal motions. The figure shows that the rising branch of the Walker circulation is centered on 125˚ E, while the sinking branch is spread across a wide region between the dateline and 80˚ W. Within this region, westerlies are present between 100 and 400 mb, and easterlies are confined below 700 mb. Upper-level easterly flow exists between 120˚E and 160˚E, and appears to be associated with the Australian winter monsoon. The flow is quite weak between 400 and 700 mb. NKVB also described additional cells in the equatorial plane which Bjerknes did not mention. Their data (not shown) indicated the presence of Walker-like circulations over the tropical Atlantic ocean, near the African sector, and the western branch of the Pacific Walker cell.

Fig. 11.4 shows that the 1000-mb winds above the tropical Pacific (between 10˚ N and 10˚ S) have an easterly component in both solstitial seasons. For both seasons, easterly flow near the equator occurs west of about 90˚ W. In January, the easterly component is particularly strong above the central equatorial Pacific, and convergence is evident along the ITCZ near 8˚ N. In July, a notable characteristic is the strong cross-equatorial flow in the eastern Pacific. The zone of convergence at 1000 mb during the NH summer has moved north

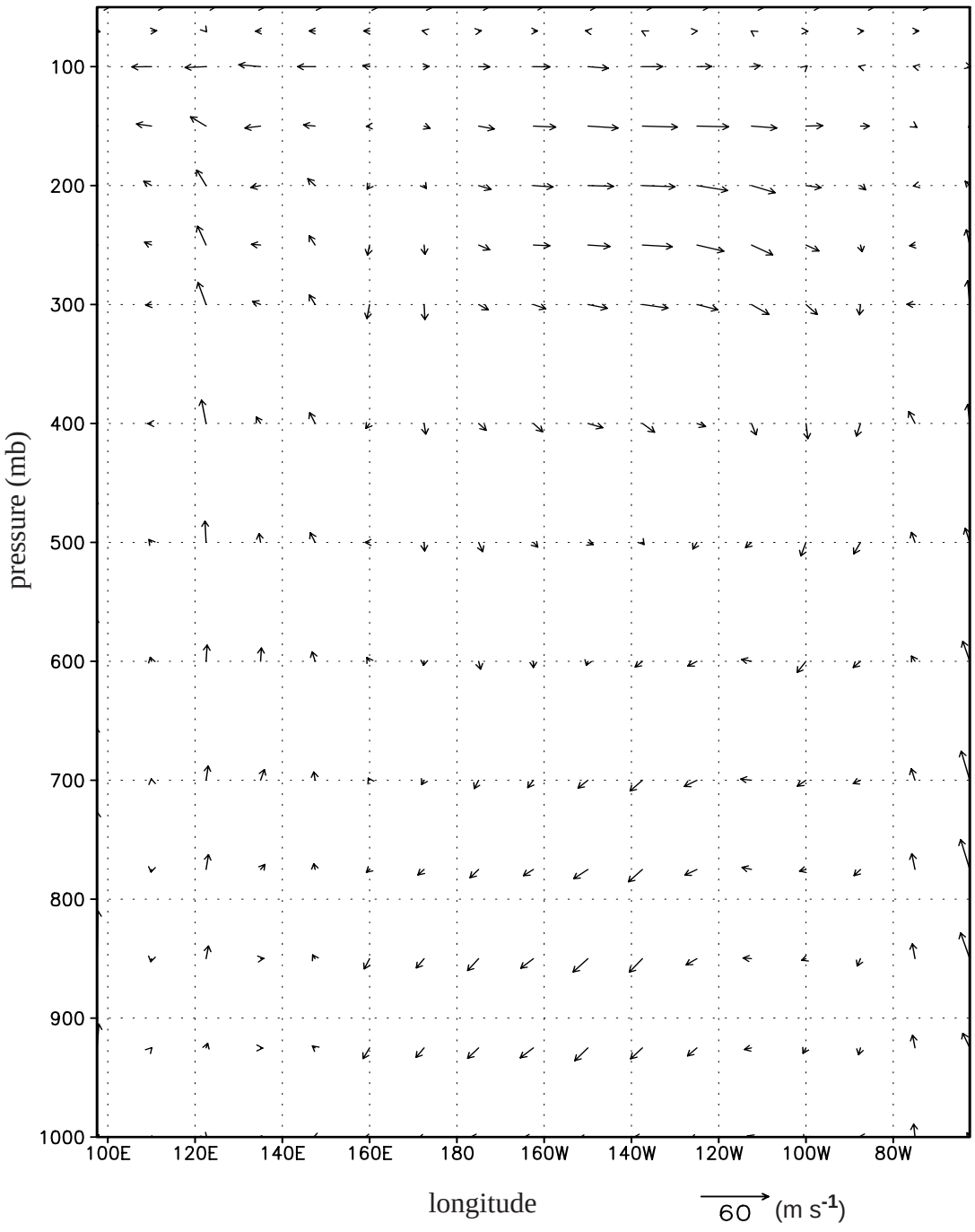

Figure 11.3: January 1989 Equatorial u–ω vectors in units of m s^{-1}. The ω values, which were originally in units of Pa s^{-1}, were scaled by –300 m Pa^{-1}.

of 10˚ N over the eastern Pacific. At the latitude of the ITCZ, the easterly fetch originates to the east of Central America during both seasons. If we consider the Walker circulation to occur at near-equatorial latitudes, then easterly flow at 1000 mb cannot originate over the continents because the mountains of Peru act as a vertical barrier on the eastern boundary of the ocean. However, we note that a strong southerly component is evident during both seasons.

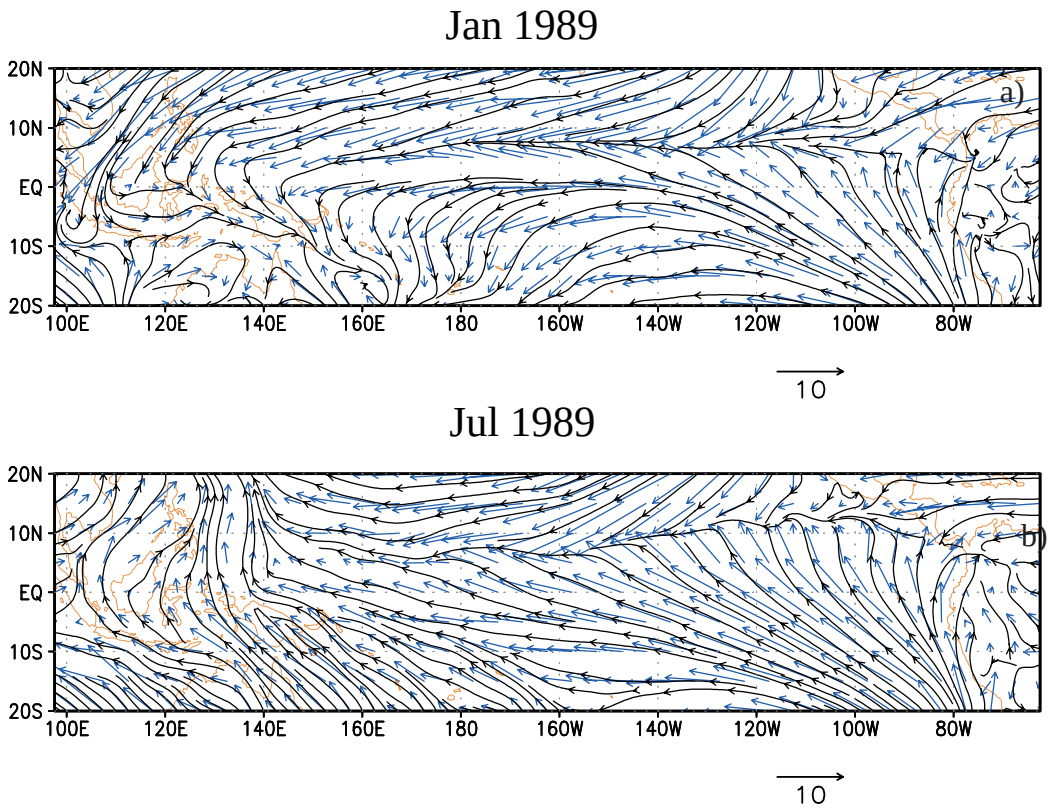

Figure 11.4: Streamlines and horizontal wind vectors for the tropical Pacific at 1000 mb for a) January 1989 and b) July 1989. The units are m s^{-1}.

Lindzen and Nigam (1987) used a simple model to show that SST gradients are capable of forcing low-level winds and convergence in the tropics. They assumed that near the surface the Coriolis acceleration is balanced by the sum of the horizontal pressure-gradient force and wind stress; this is called an Ekman balance. Linearizing about a state of rest, they found a pressure field that qualitatively resembles the observations, although the wind speeds were unrealistically strong. Neelin et al. (1998) show that the model used by Lindzen and Nigam (1987) is very similar to that of Gill (1980).

Newell et al. (1996; hereafter N96) compared water-vapor data from the Upper Atmosphere Research Satellite (UARS) with upper-air wind data from the ECMWF reanalysis dataset to deduce horizontal and vertical motions in the tropical atmosphere. Their results indicate regions of strong ascending motion over the western Pacific Warm Pool and the South Pacific Convergence Zone. The main regions of sinking motion, which are located off South America and extend westward to the dateline just south of the equator, exhibit little

seasonal movement. For comparison, Fig. 11.6 shows the vertical velocity fields at 300-mb

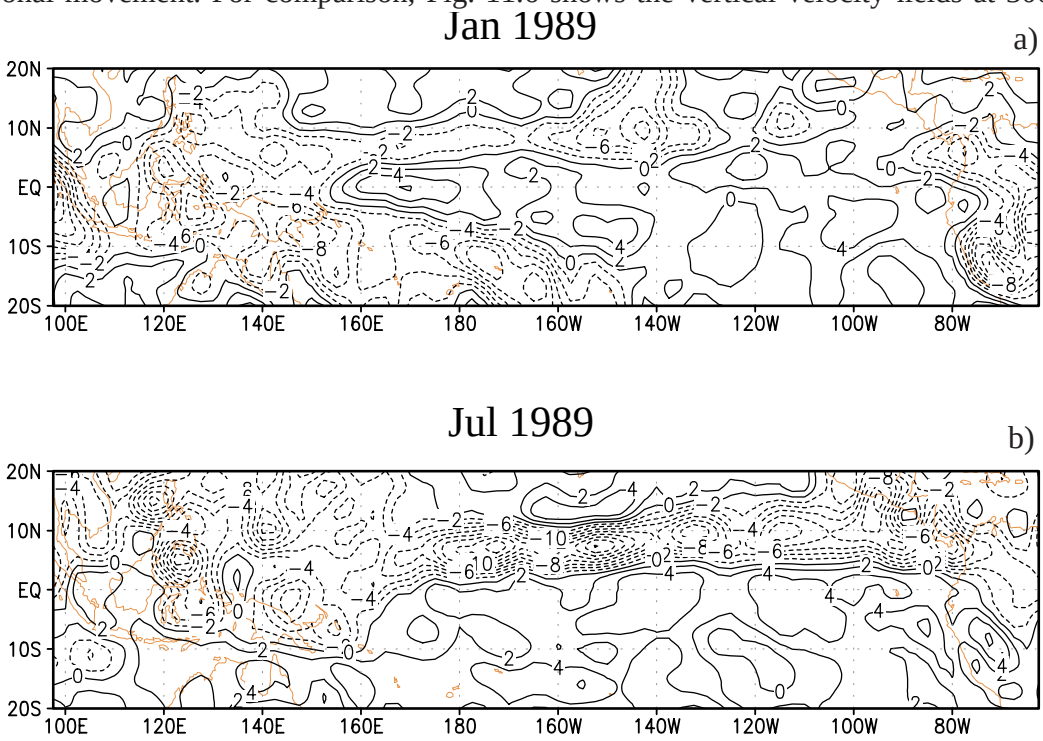

Figure 11.5: Contour plot of mean vertical velocity at 300mb (units, 10^{-2} Pas^{-1}) from the ECMWF reanalysis dataset for a) January 1989 and b) July 1989. Contour interval is 2 x 10 $^{-2}$ Pa s^{-1}; negative contours are dashed. Data were obtained from NCAR.

from the ECMWF reanalysis dataset for the solstitial months. During January 1989, centers of ascending motion were located near 145˚ E at latitudes 5˚ N and 5˚ S. The SPCZ is clearly evident in the January 1989 data, with a large region of ascending motion that extends southeastward from 145˚ E to 160˚ W. A region of strong sinking motion straddles the equator and extends eastward from 160˚ E. During July 1989, the ascending region remains fixed at 145˚ E, but the NH and SH centers of ascending motion have merged on the equator. During the NH summer, the ITCZ is well developed at 5° N, and so the zone of sinking motion has slipped southward from its January position, particularly the zone over the central Pacific. The general pattern is one in which ascending motion dominates over the tropical western Pacific, while sinking motion occurs over the tropical central and eastern Pacific. Easterlies extend across the equatorial Pacific from South America to 170˚ W and 160˚ E. West of 160˚ E, the low-level equatorial winds are very weak. However, easterlies span the equatorial Pacific at 5° S and 5° N.

Fig. 11.6 shows the upper branch of the Walker circulation. West of the dateline, the zonal winds over the equator are easterly. Upper-level westerly flow occurs to the east of the rising motion. During July 1989, the upper-level flow above the equatorial Pacific ocean is entirely from the east. In the northern hemisphere (NH), weak westerly flow appears between 170˚ W and 140˚ W poleward of 15˚ N. In the southern hemisphere (SH), a westerly component of the wind exists south of 5˚ S to the east of the dateline. An interpretation is that

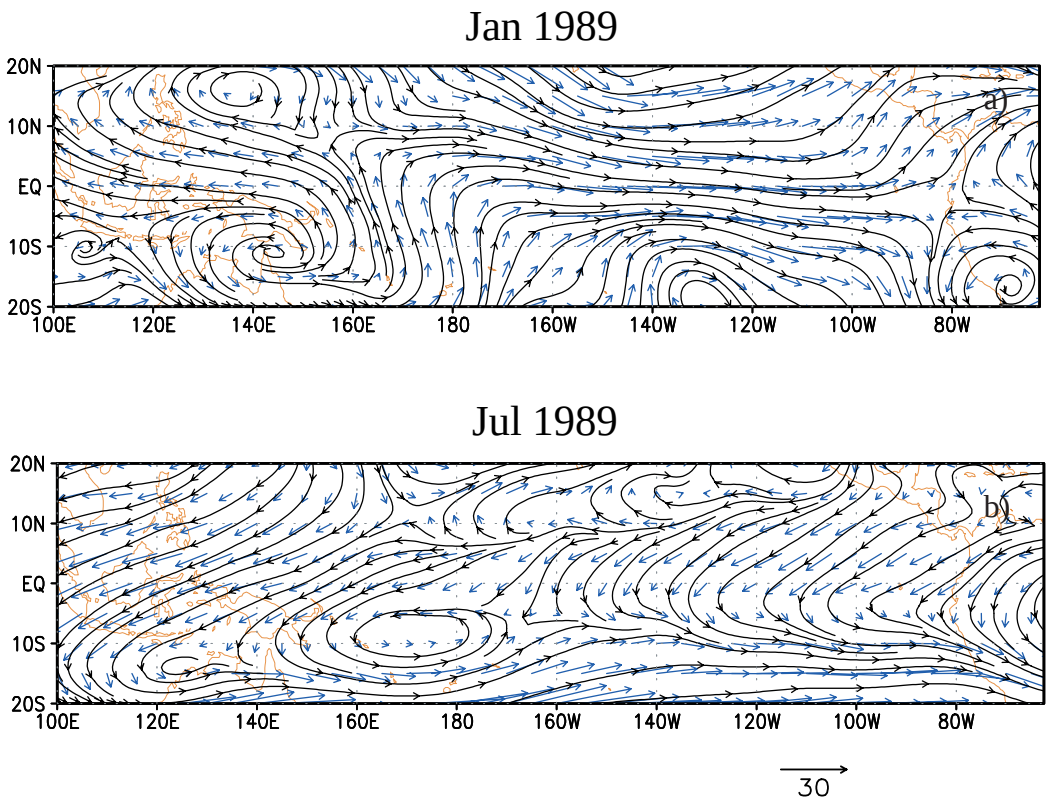

Figure 11.6: Streamlines and horizontal wind vectors for the tropical Pacific at 200 mb for a) January 1989 and b) July 1989. The units are m s^{-1}.

the Walker circulation has migrated into the SH. A reexamination of Fig. 11.5b indicates that sinking motion is confined mainly to the SH, and occurs as far west as 165˚ W.

11.3 The relationship between the Walker Circulation and the sea surface temperature.

The Walker Circulation is an atmospheric phenomenon, so you may be wondering why we discuss it in detail in a chapter dealing with atmosphere-ocean interactions. The reason is that the Walker Circulation is closely tied to east-west sea surface temperature gradients which are produced by atmospheric phenomena including aspects of the Walker Circulation itself. The Walker Circulation can thus be viewed as a phenomenon of the coupled atmosphere-ocean system.

Fig. 11.7 shows that a sea-surface temperature (SST) maximum occurs over the tropical region centered on 120˚ E, and for this reason the region is known as the tropical Warm Pool. The “cold tongue” is a band of relatively cold waters along the equator that stretches from South America westward to near 160˚ E. Although a noticeable SST gradient exists along and across the cold tongue, the temperature variation is still much smaller than that which is generally observed in extratropical or polar regions of the globe. The tropical climate is characterized by sea surface and horizontal air temperature gradients which are weak compared to the corresponding mid-latitude gradients. As explained by Charney (1963), for cloud-free regions of the tropics, pressure and temperature gradients must be small compared to those of midlatitudes.

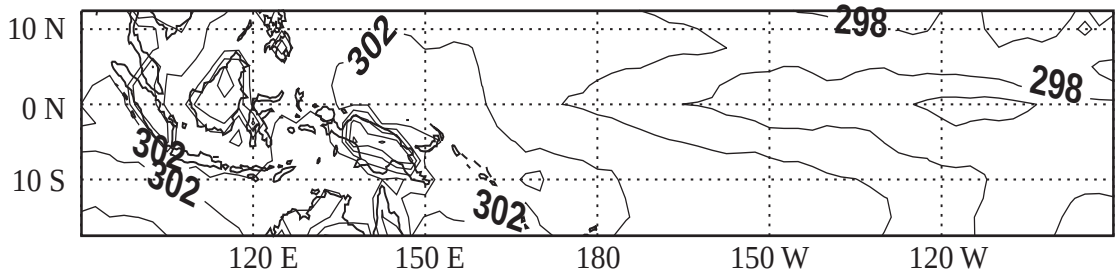

Figure 11.7: Tropical skin temperature for January 1989 from the ECMWF reanalysis dataset obtained from NCAR. Resolution for this dataset is 2.5° and the contour interval is 2 K.

The distribution of tropical convection is strongly related to both the local SST and the SST gradient. The tropical-Pacific Warm Pool is a region of intense deep convection. In Fig. 11.8, regions in which the outgoing longwave radiation (OLR) is less than 225 W m^{-2} can be identified as areas of frequent convection (Webster 1994). The OLR threshold corresponds to a monthly mean emission temperature of 250 K. Due to longwave trapping by optically thick anvil clouds, which are produced by deep convection, the OLR is reduced and threshold values of OLR can therefore be used as surrogates to infer the presence of convection. From

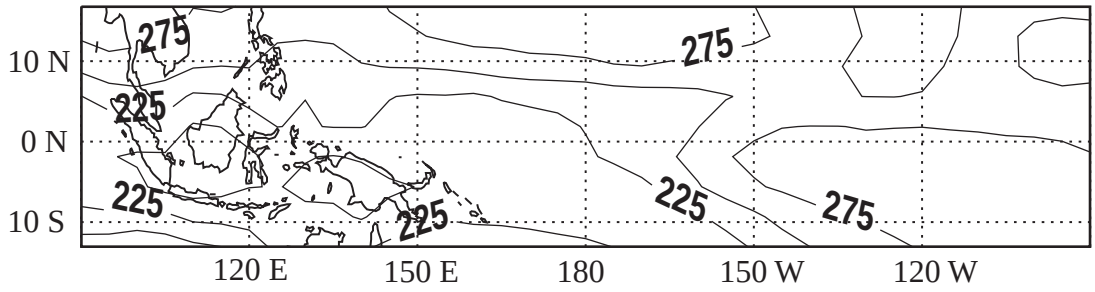

Figure 11.8: Tropical OLR for January averaged over 1985 to 1988. Daily means from the Earth Radiation Budget Experiment (ERBE) were averaged and interpolated onto a 5° × 4° (longitude–latitude) grid. The units are W m^{-2}.

the figure, we see that convection occurs throughout the Warm Pool, and in the South Pacific convergence zone (SPCZ). On the other hand, the OLR is generally larger than 275 W m^{-2} across the equatorial cold tongue, indicating that convection is infrequent there.

Ramanathan and Collins (1991) hypothesized that cirrus clouds act as a thermostat to regulate tropical SST. They used Earth Radiation Budget Experiment (ERBE) data to deduce the inter-relationships among shortwave and longwave cloud radiative forcings and radiative forcing of the clear atmosphere. They emphasized that the shortwave effects of clouds dominate over the longwave effects in regulating SST. According to their hypothesis, as SST increases, the cloud albedo increases. According to their idea, the atmosphere warms as a result of longwave cloud radiative effects, stronger latent-heat release by convection, and a stronger SST gradient over the tropical Pacific. This warming leads to an amplification of the large-scale flux convergence of moisture. The process continues until the reflectivity clouds increases sufficiently to cool the surface. A criticism of their study is that changes in the

strength of the ocean and atmosphere circulations were not included. Nevertheless it undoubtedly true that the blocking of shortwave radiation by deep cloud systems tends to limit the sea-surface temperature in the Warm Pool.

In the eastern tropical Pacific, stratus clouds in the boundary layer intercept sunlight and strongly reduce the heat flux into the ocean below (e.g. Hartmann et al. 1992). In this way, the atmosphere helps to maintain the cooler SSTs of the eastern Pacific. Stratus clouds form preferentially over cold water (Klein and Hartmann 1993), so a positive feedback is at work here (Ma et al. 1996). Latent heat exchange between the ocean and atmosphere is influenced by the surface relative humidity and the surface winds. For fixed relative humidity and SST, the evaporative cooling of the ocean increases as the surface wind stress increases. The winds also influence the SST distribution by generating cold-water upwelling in the eastern Pacific, and along the equator in the eastern and central Pacific. The equatorial cold tongue is an example of an effect of cold-water upwelling on the SST distribution.

11.4 Theories of the Walker Circulation

The driving force behind the Walker circulation is the zonal structure of the precipitation rate, and that these variations are balanced by adiabatic heating/cooling due to sinking/rising motions. Over the warm waters of the western Pacific, latent heat release due to intense convection is balanced by adiabatic cooling and ascending motion (Webster 1987). The deep, bright clouds limit the radiative cooling of the atmosphere over the Warm Pool. It is the inability of radiative processes to *locally* balance the latent heating which gives rise to a tropical circulation. Over the eastern tropical Pacific, where the SST is relatively cold, convection is infrequent, and so a balance between radiation and subsidence exists.

Pierrehumbert (1995; hereafter P95) presented a two-box model of a Hadley/Walker circulation which has strongly influenced recent studies of the tropical climate. Fig. 11.10 presents a schematic of the furnace/radiator-fin model in P95. The model has separate energy budgets for its Cold-Pool and Warm-Pool regions. SSTs for the Cold Pool and Warm Pool were constrained to be those which give energy balance for each box of the model atmosphere and for the Cold-Pool ocean. Surface energy balance for the Warm Pool was not explicitly included in the model, even though it was discussed in detail. A vertically and horizontally uniform lapse rate was assumed, and the free-tropospheric temperature profile was assumed to be uniform across the tropics. The radiating temperature of the Cold-Pool free atmosphere was assumed to be the air temperature at $z = z_T/2$, where z_T is the assumed height of the tropopause. The solution was obtained by first computing the net energy flux at the top of the Warm-Pool atmosphere for a given SST and relative humidity profile. The net radiative flux at the Warm-Pool TOA was assumed to be balanced by a horizontal energy transport to the Cold Pool. The Cold-Pool SST and radiating temperature were then computed under the constraint that the net diabatic cooling must balance the energy imported laterally from the Warm Pool.

The mass flux was assumed to be that required to give a balance between adiabatic warming by dry subsidence and the net radiative cooling of the Cold-Pool region. The mass flux is proportional to the sum of the net diabatic cooling of and specified mid-latitude atmospheric energy transport from the Cold Pool. The potential temperature difference between the inflow and outflow regions of the Cold-Pool atmosphere was specified. Therefore, the mass flux responds only to changes to the net diabatic cooling of the Cold Pool. Because precipitation over the Cold Pool is neglected, the diabatic cooling of the Cold-Pool atmosphere is purely radiative and depends on the Warm-Pool and Cold-Pool SSTs, and on the emissivity of the Cold-Pool atmosphere, which is a prescribed parameter. P95 assumed a uniform vertical temperature profile for the atmosphere which is controlled by

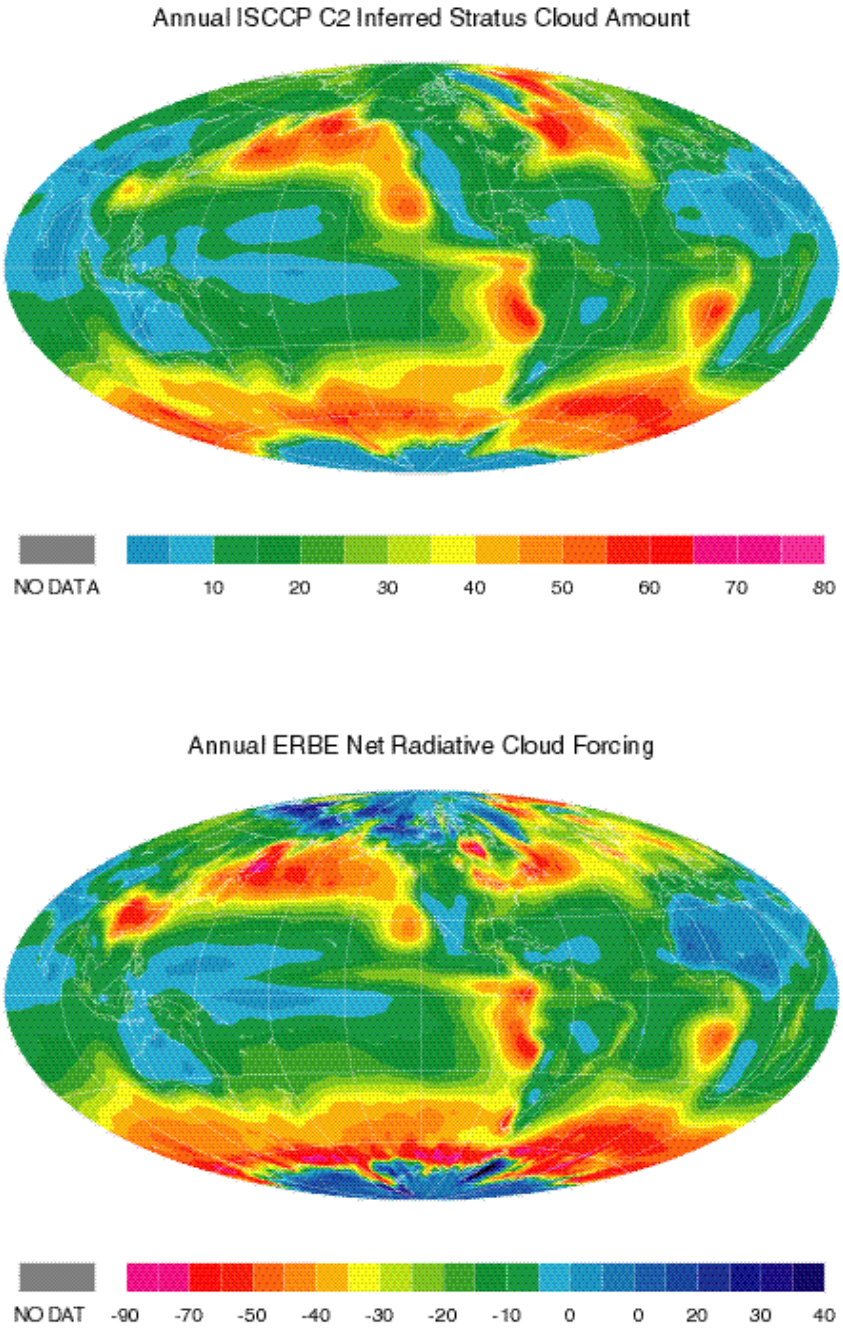

Figure 11.9: Observed annual-mean low-cloud amount (upper panel) and the net effects of clouds on the Earth's radiation budget (lower panel). Negative values in the lower panel indicate a cooling, i.e. shortwave reflection dominates longwave trapping.

Warm-Pool SST, and so the radiating temperature of the Cold-Pool atmosphere depends on

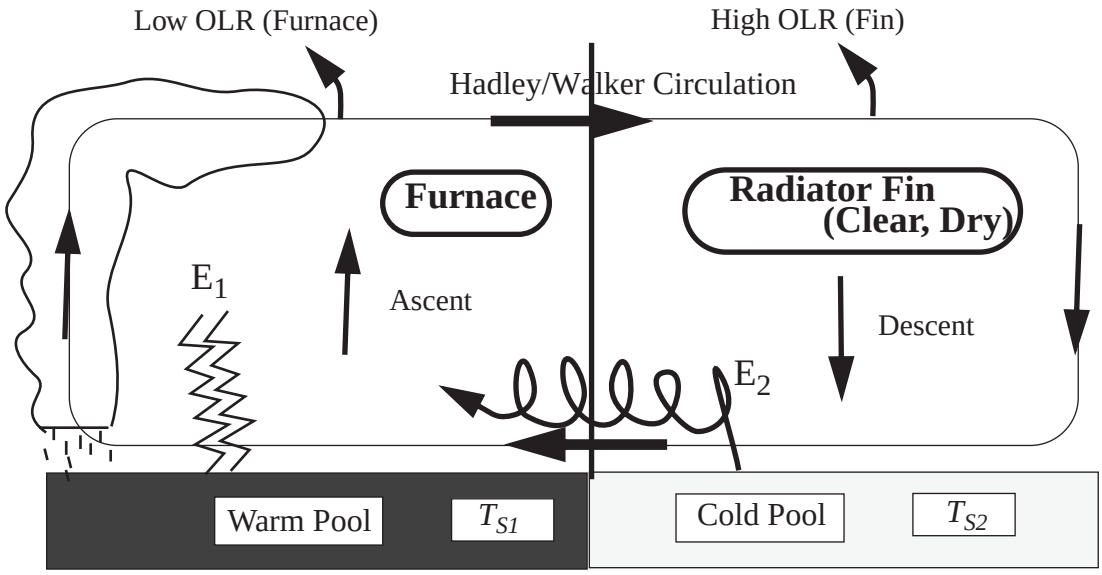

Figure 11.10: Reproduction of Pierrehumbert's schematic representation of the 'furnace/radiator–fin' model of the tropical circulation. The symbols E and TS represent the evaporation rate and SST, respectively. The subscripts 1 and 2 denote the Warm Pool or furnace and the Cold Pool or radiator fin.

Warm-Pool SST. It can be shown that the horizontal heat transport by the Warm-Pool atmosphere, F_{ah1}, is proportional to the diabatic cooling of the Cold-Pool atmosphere and to the ratio of Cold-Pool area, A_2, and Warm-Pool area, A_1. This ratio is also a prescribed parameter of the model.

The column energy budget for the model is given by

$$H = (Q_{v1} + F_{a\exp})\frac{A_1}{A_1 + A_2} + (Q_{v2} + F_{a\exp})\frac{A_2}{A_1 + A_2}, \tag{11.1}$$

where Q_v is the energy added to the Cold-Pool atmospheric column due to vertical flux convergence and F_{aexp} is the specified, horizontal-mean, net horizontal, atmospheric energy transport into the column. The radiative effects of clouds were ignored. In equilibrium, $H = 0$, and so

$$(Q_{v1} + F_{a\exp})A_1 + (Q_{v2} + F_{a\exp})A_2 = 0. \tag{11.2}$$

For the case in which $F_{aexp} = F_{oh1} = F_{oh2} = 0$, where F_{oh} is the horizontal energy transport by the ocean, the net horizontal, atmospheric heat transport for the Warm Pool is given by $F_{ah1} = -Q_{v1}$. Obviously, F_{ah1} increases as the ratio A_2/A_1 increases for a fixed Cold-Pool radiating temperature, and the climate cools for a fixed radiating temperature. P95 argued that Q_{v1} is bounded due to limits on the OLR in moist atmospheres, i.e. the increase of OLR

with SST levels off due to the longwave-trapping effect of water vapor, which also increases with SST. As A_2 becomes much larger than A_1, the horizontal energy transport between boxes must vanish, and radiative equilibrium results. For small A_2/A_1, Q_{v2} is not bounded because the radiative temperature of the Cold Pool can be increased as much as needed in order to yield a finite energy transport between boxes, no matter how small A_2 becomes. Since the Warm-Pool SST controls the Cold-Pool radiating temperature, the Warm Pool becomes extremely hot in this limit.

P95 also showed that for very small values of the Cold-Pool emissivity, the Warm-Pool SST runs away, because the Cold Pool cannot radiate enough energy to balance the Warm Pool. This is called a runaway greenhouse (Ingersoll 1969). As the Cold Pool's emissivity is increased, the SSTs of the Warm Pool and Cold Pool decrease and increase, respectively.

For fixed, lateral atmospheric energy transport, a larger A_2/A_1 implies a smaller Q_{v2}, which can be seen from (11.2). It can be shown that a smaller Q_{v2} leads to a reduced Cold-Pool mass flux. Because the Cold-Pool mass flux was assumed to be proportional to the Cold-Pool surface evaporation rate, increasing A_2/A_1 warms the Cold-Pool SST. On the other hand, as the Cold-Pool emissivity increases, the radiating temperature of the Cold-Pool atmosphere must decrease in order to radiate the same amount of energy. Because the Warm Pool controls the temperature profile, its equilibrium SST must decrease as the Cold-Pool radiating temperature decreases. As the Cold-Pool emissivity increases, the Warm-Pool cools off. The simulated Cold-Pool and Warm-Pool SSTs resemble the present-day climate for a range of conditions. The diagnosed Cold-Pool mass flux is realistic. A serious weakness of the model is that it fails to account for cloud-radiative effects in the Warm-Pool region.

Next, we discuss an appealingly simple box model developed by Sun and Liu (1996; hereafter SL) to demonstrate the role of dynamic ocean-atmosphere coupling in SST regulation. SL constructed a three-box model (Fig. 11.11) of the tropical Pacific ocean, which is coupled to a very simple model atmosphere. Two adjacent equal-volume boxes represent the surface layer of the eastern and western Pacific ocean regions, respectively, and a sub-surface box represents the equatorial undercurrent. Water is assumed to be advected into the western box from the eastern box, which is fed by upwelling of the equatorial undercurrent. Water returns to the equatorial undercurrent by subduction from the western box. The temperature of the equatorial undercurrent, T_c, was specified based on observations. The temperature tendencies for the two surface-layer boxes are assumed to be controlled by dynamical ocean-atmosphere processes and by thermal advection in the ocean. SL crudely parameterized the dynamical processes as a relaxation toward an equatorial equilibrium temperature T_e, with inverse time scale c. In order to determine T_e, the feedbacks due to surface emission, the clear-sky greenhouse effect, the greenhouse effect of clouds, and the cloud shortwave forcing with respect to an SST perturbation at T_0 = 300 K (i.e. the partial derivatives) were estimated. Except for the value of the surface emission feedback which is easily calculated, values for the other feedbacks were taken from published estimates. The difference between T_e and T_0 was then computed by taking the quotient of the net heating of the ocean-atmosphere column which was evaluated at T_0 and the summed feedbacks for an SST perturbation. The advective temperature tendency can be shown to be proportional to the temperature difference between water entering and departing each box. The advection proportionality parameter, q, was assumed in turn to be proportional to the temperature difference between the two surface boxes, with a specified constant of proportionality, α. Thus, the advective temperature tendencies for the Warm and Cold Pools are given by $\alpha(T_1$-

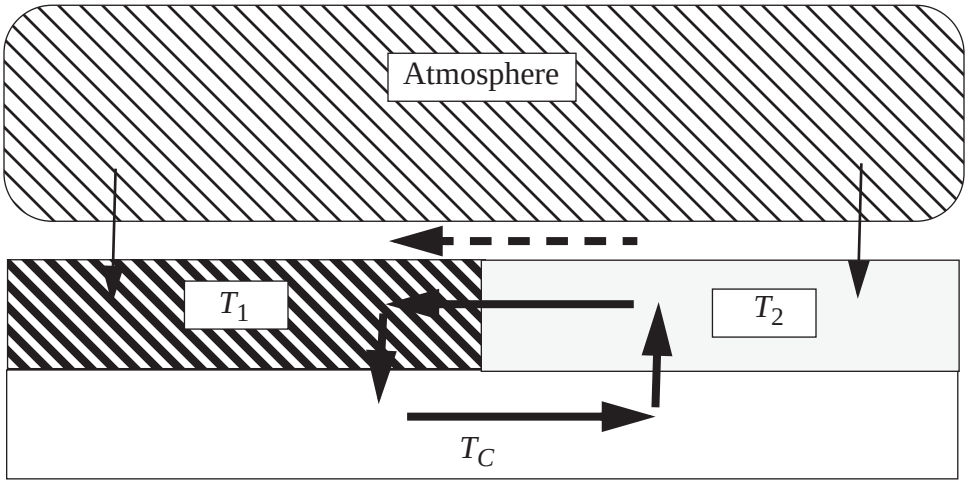

Figure 11.11: Schematic of the Sun–Liu coupled model. The boxes represent the atmosphere (light hatching), the Warm Pool (heavy hatching), the Cold Pool (stippling), and the undercurrent (clear box). Heavy arrows denote ocean currents, light arrows denote local heating and the dashed arrow represents the surface winds.

$T_2)^2$ and $\alpha(T_1\text{-}T_2)(T_c\text{-}T_2)$, respectively. The rationale for this form of q is that the strength of the ocean currents is proportional to the surface wind speed, which is assumed to be proportional to the east-west SST gradient.

SL found that the solution of their model is completely determined by a non-dimensional parameter $\beta = (\alpha/c)(T_e - T_c)$, which gives the strength of the dynamic coupling relative to the thermodynamic forcing. As seen in Fig. 11.12, the east-west SST gradient and the ocean currents are zero for $\beta < 1$, and hence the tropical Pacific ocean-atmosphere column is in radiative-convective equilibrium, with equilibrium temperatures $T_1 = T_2 = T_e$. This contrasts with the results of P95 which show that, due to the strong greenhouse effect, the Warm-Pool ocean-atmosphere column cannot establish radiative-convective equilibrium unless the SST is very warm and the atmosphere is very dry. For $\beta > 1$, two solutions exist. The radiative-convective solution still holds, but is unstable to perturbations. As a numerical integration of the model shows, a perturbation of the radiative-convective equilibrium causes the system to evolve to the second solution, which features a finite east-west temperature difference. The SSTs of the two surface boxes are colder than the radiative-convective equilibrium. As shown in Fig. 11.12, ocean currents develop for $\beta > 1$, and advection of undercurrent water to the Cold Pool and Cold-Pool water to the Warm Pool leads to colder SSTs in the Cold Pool and Warm Pool, respectively. The "Warm" Pool becomes warmer than the "Cold" Pool because water advected from the Cold Pool to the Warm Pool is warmer than water upwelled to the Cold Pool from the undercurrent. As described in Liu and Huang (1997), this destabilization of the radiative-convective equilibrium can be interpreted as a wind-cold water upwelling positive feedback. SL argue that T_e increases and c decreases due to positive radiative feedbacks in the atmosphere, such as those from water vapor and clouds. Since β increases with increasing T_e and decreasing c, SL assert that strong positive feedbacks of the atmosphere play a role in the evolution of the

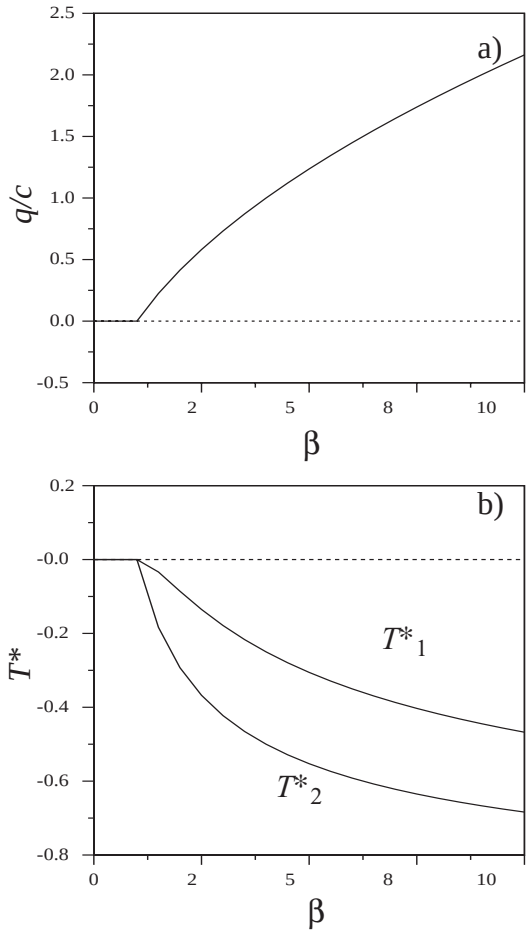

Figure 11.12: The Equilibrium solution from the Sun–Lu coupled model for (a) current strength measuered by q/c, and for (b) non–dimensionalized SST as given by $T^*_1 = (T_1 - T_e)/(T_c - T_e)$ **and** $T^*_2 = (T_1 - T_e)/(T_c - T_e)$ **, as functions of** β**.**

system from radiative-convective equilibrium. The ocean circulation transports heat from the subsurface to surface ocean, and leads to cooler SSTs. SL also showed that as T_e increases, the difference between Warm-Pool SST and T_e increases. This represents a regulation of the Warm-Pool SST, and does not explicitly depend on an atmospheric circulation. Results from a simplified coupled ocean-atmosphere general circulation model (GCM) support these conclusions.

Miller (1997; hereafter M97) extended Pierrehumbert's model by studying the radiative effects of low clouds in the Cold-Pool region. Extending the basic concepts of P95, Miller constructed a three-box model, which includes energy- and moisture-balance equations for the boundary layer and free troposphere and a surface energy budget for each of three boxes: the updraft region, the Warm Pool, and the Cold Pool. Taking advantage of the small surface area covered by the updrafts, M97 simplified the model for the limit of vanishing updraft surface area. M97 demonstrated that in this limit, the boundary layer and tropopause of the Warm Pool region must be connected by a moist adiabat. Miller assumed that the lapse

rate of the Warm Pool region is moist adiabatic. Following P95, atmospheric dynamics were implicitly included by assuming a uniform free-tropospheric temperature sounding across both the Warm and Cold Pool regions.

The main finding of M97 is that low clouds act as a thermostat for tropical SST. Without a realistic distribution of stratus clouds, the SST was too warm beneath the subsiding branch of the tropical circulation. Although low clouds reduce the surface-absorbed solar radiation locally, M97 also found that the temperature drop in the Warm Pool region was nearly as large as that in the Cold Pool region. In order to obtain a realistic Warm-Pool SST, an additional -5 W m^{-2} forcing for the Cold Pool, and -12 W m^{-2} forcing for the Warm Pool were needed. This suggests that additional cloud types contribute to the surface forcing. In contrast, cloud radiative forcing was not required for the model of P95 to simulate realistic SST. This discrepancy suggests that the crude radiative transfer parameterization adopted in P95 likely canceled the impact of not including cloud radiative effects.

11.5 El Niño and the Southern Oscillation

Many studies have explored the processes that cause SST anomalies to develop in the tropical Pacific ocean (Cane and Zebiak 1985; Zebiak and Cane 1987; Battisti 1988; Battisti and Hirst 1989; Neelin and Jin 1993; Anderson and McCreary 1985; Schopf and Suarez 1988: Yamagata and Masumoto 1989; Graham and White 1990; and many others). The phenomena of El Niño and the closely related Southern Oscillation have been beautifully discussed in the book of Philander (1990).

The Southern Oscillation is a systematic shifting of atmospheric mass, back and forth

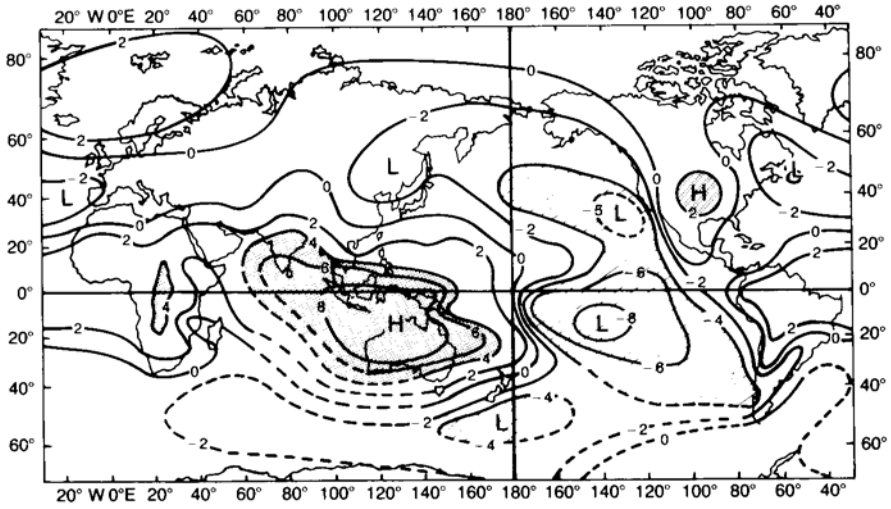

Figure 11.13: The Southern Oscillation. From Philander (1990).

across the Pacific basin. It is illustrated in Fig. 11.13, which shows the correlation of the surface pressure at various locations in the Pacific basin with the surface pressure in Darwin. A large-scale dipole structure is clearly evident. Fig. 11.14 shows year-to-year variations in the sea-level pressures measured at Darwin and Tahiti; they are generally anticorrelated.

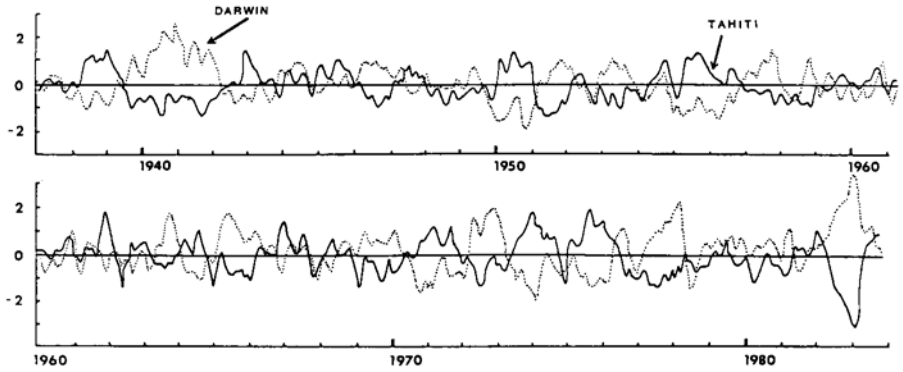

Figure 11.14: Time series of sea level pressure at Darwin and Tahiti. From Philander (1990).

In parallel with these sea-level pressure changes, we see fluctuations of the sea-surface temperature, as shown in Fig. 11.15. In certain years, the SST in the eastern Pacific is

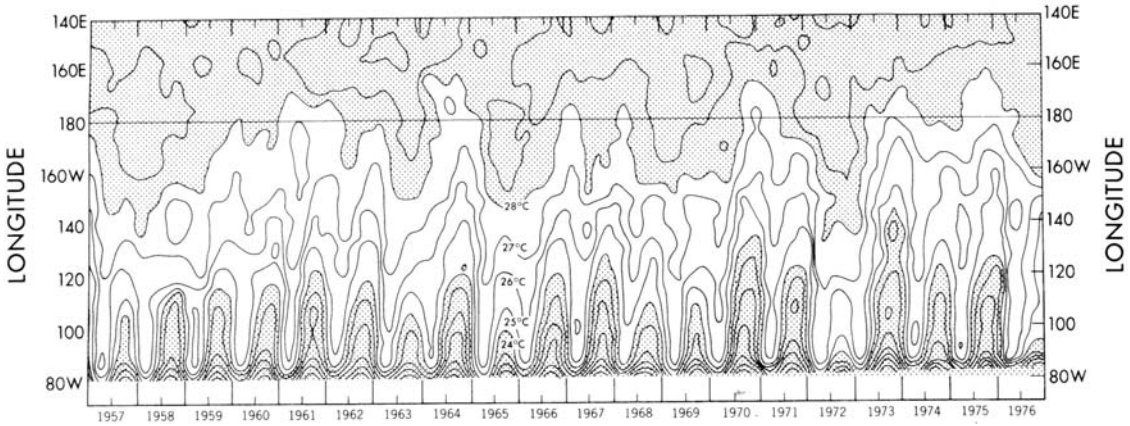

Figure 11.15: Longitude–time section of the sea surface temperature. From Philander (1990).

anomalously warm; these are called El Niño events. They tend to begin late in the calendar year. We also see some years with anomalously cold temperatures in the eastern Pacific; these are called La Niña events. El Niños are associated with weak upwelling west of South America, and La Niñas are associated with strong upwelling. In some cases, the SST anomalies tend to move westward, as would be expected given the eastward currents driven by the trade winds.

As shown in Fig. 11.16, there are also very strong year-to-year variations of the precipitation in various locations. Heavy precipitation in the central and eastern Pacific is generally correlated with anomalously light precipitation in the western Pacific. In El Niño years, the east is wet and the west is dry.

Fluctuations of the SST in 1982 and 1983 are shown in Fig. 11.17. These years saw a very strong El Niño. See also Fig. 11.18. During the El Niño, the cold tongue of water along

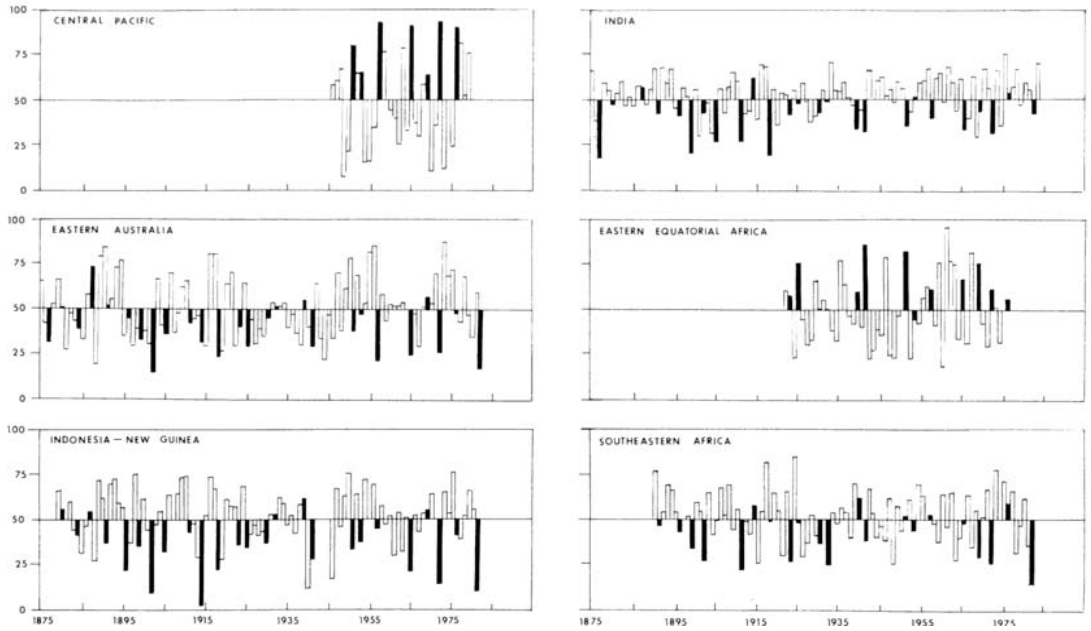

Figure 11.16: Time series of precipitation at selected locations. The black bars are El Niño years. From Philander (1990).

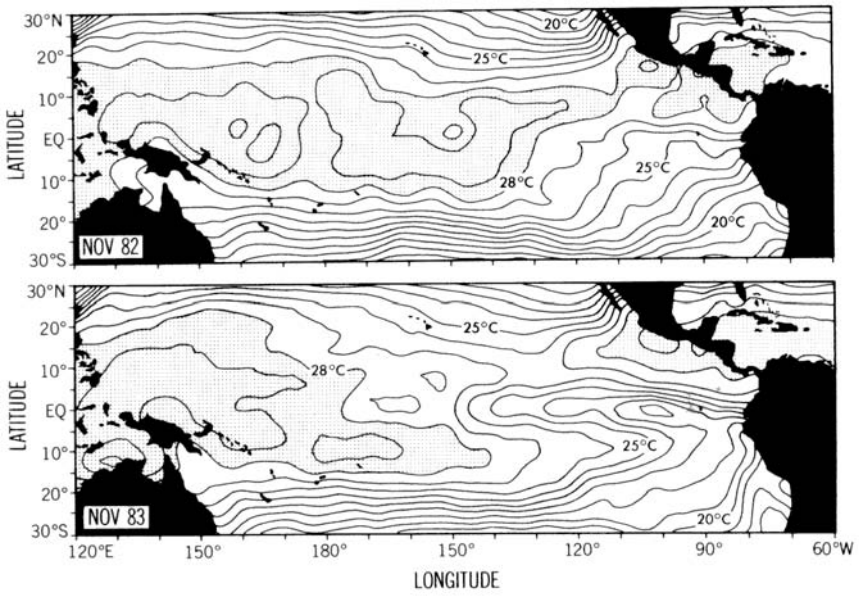

Figure 11.17: Observed SSTs for November 1982 and November 1983. From Philander (1990).

the Equator virtually disappeared. Warm water appears to migrate from east to west. On the other hand, Fig. 11.19 appears to show deep clouds migrating from west to east.

The response of the upper-tropospheric circulation to El Niño is shown in Fig. 11.20.

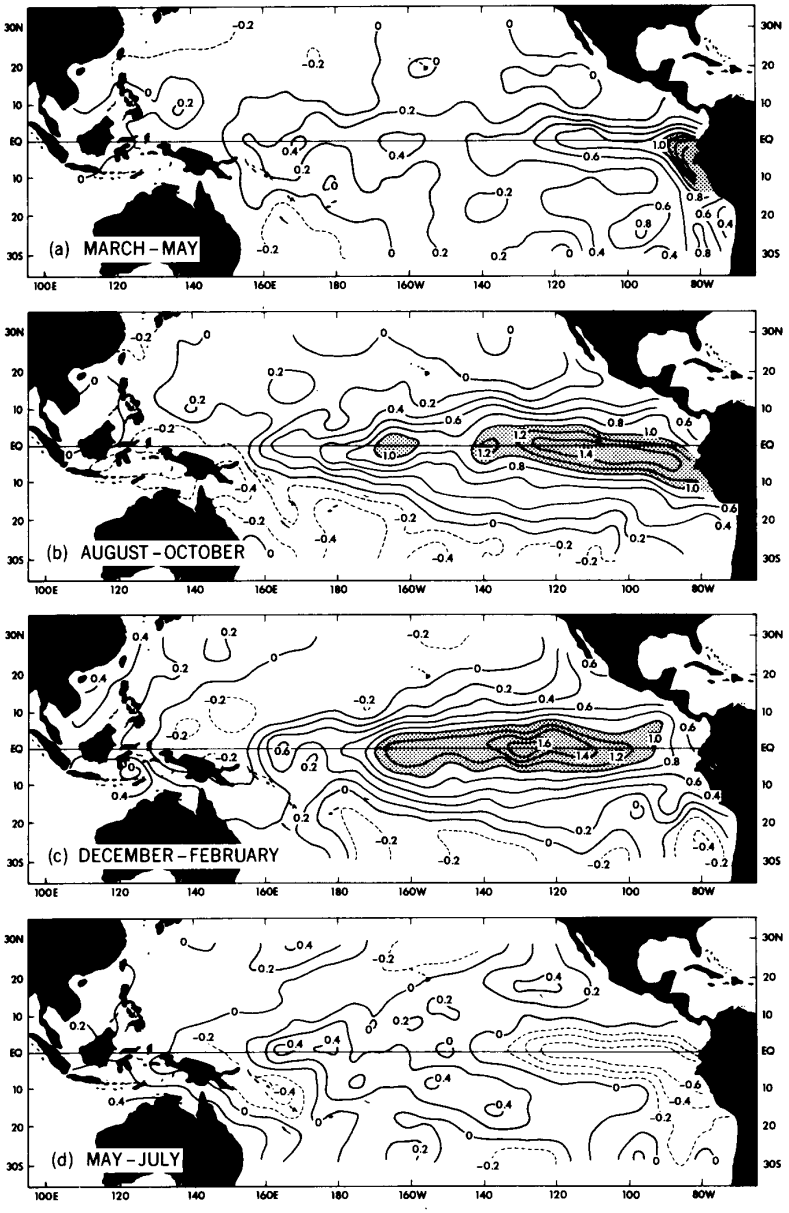

Figure 11.18: Maps of sea surface temperature anomalies during 1982 and 1983. From Philander (1990).

Twin anti-cyclones straddle the region of enhanced convection. The anticyclonic vorticity can be interpreted as a response to the divergent outflow from the convective region.

11.5.1 Sea surface temperature and thermocline slope

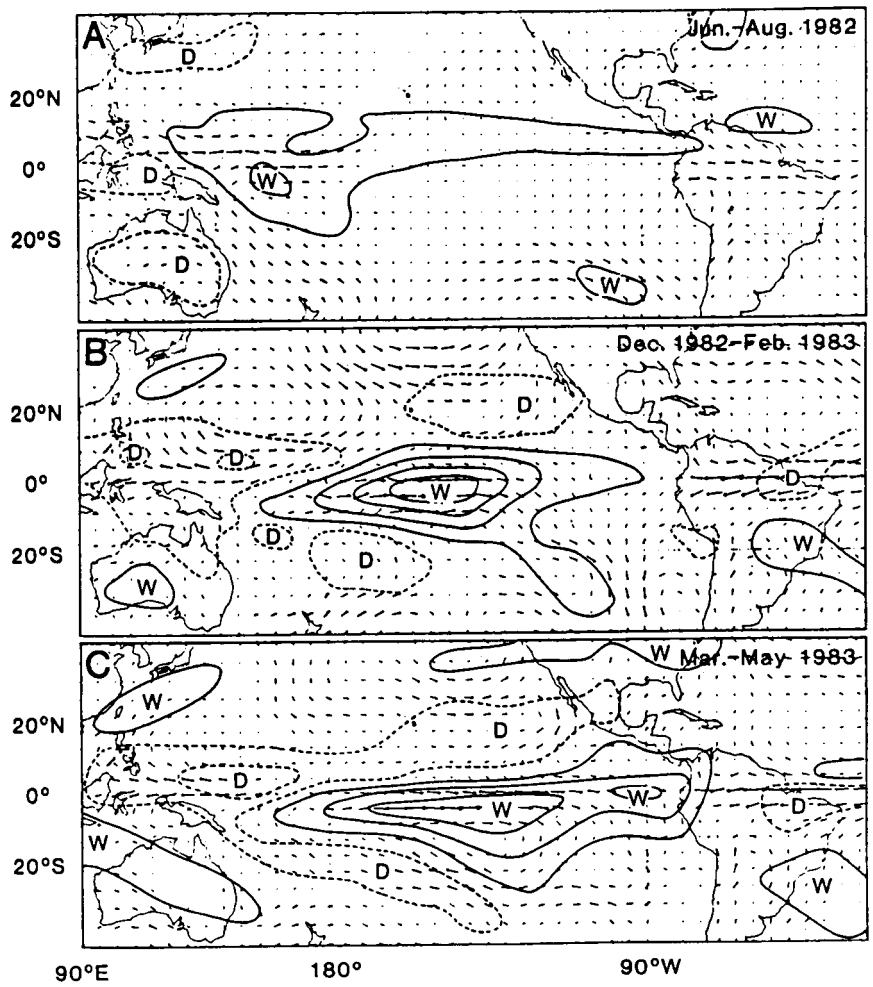

Figure 11.19:Anomalies of outgoing longwave radiation and the winds, for 19982 and 1983. From Philander (1990).

Consider the upper-ocean structure shown in Fig. 11.21. We let z_T denote the depth of the thermocline. The density jump across the thermocline is $\Delta\rho \equiv \rho_D - \rho_S > 0$. The hydrostatic equation is given by

$$dz = \frac{dp}{\rho g}. \tag{11.3}$$

There is no minus sign because both depth and pressure increase downwards. If $p = p_{ref} =$ constant at $z = z_{ref}$, and with

$$p_S \cong 0, \tag{11.4}$$

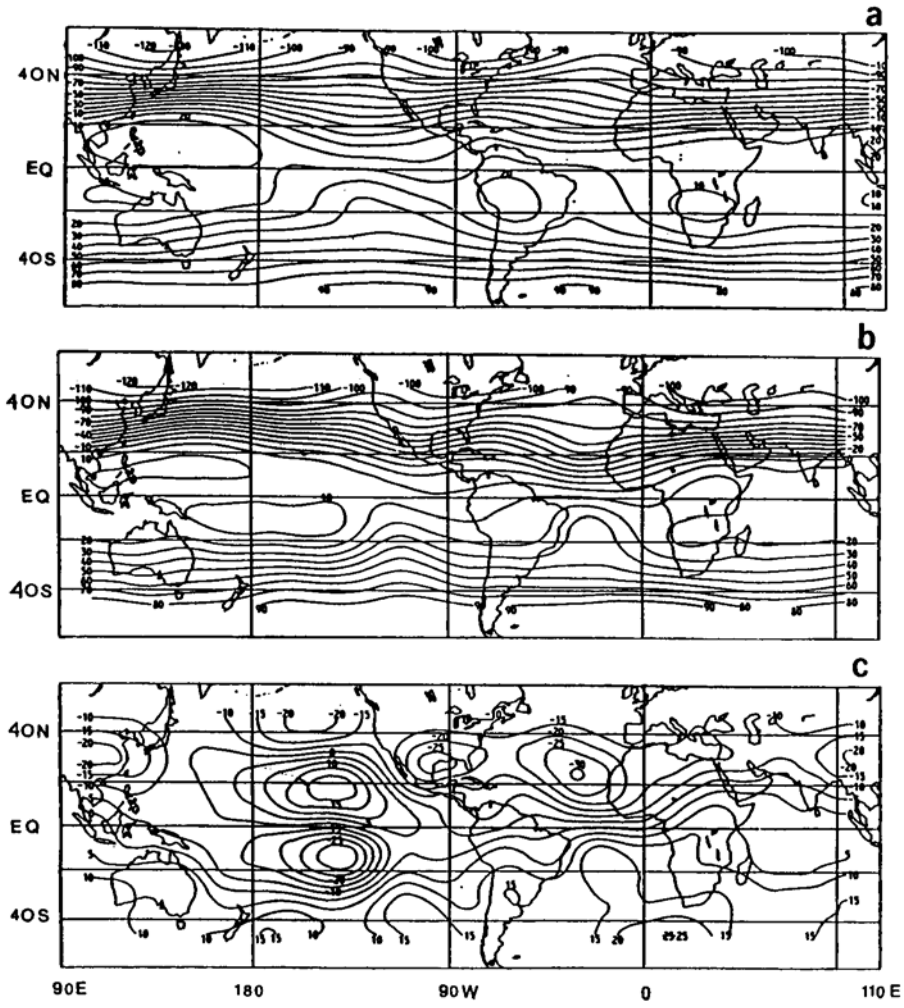

Figure 11.20: Streamfunction of the 200 mb winds. The bottom panel is a difference plot. From Philander (1990).

which means neglecting the weight of the atmosphere compared with the weight of the water in the column below, we get

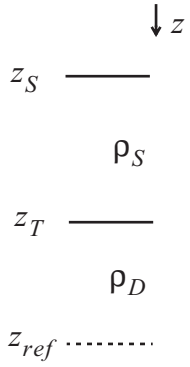

Figure 11.21: The assumed density distribution in the upper ocean. The depth, z, increases downward from zero at a level near the surface. The surface depth, z_S, is not necessarily zero; it can be slightly positive or slightly negative as sea level varies.

$$z_S = z_{ref} - \frac{1}{g}\int_o^{pref} \frac{dp}{\rho}$$

$$= z_{ref} - \frac{1}{g}\left\{\int_o^{p_T} \frac{dp}{\rho} + \int_{p_T}^{p_{ref}} \frac{dp}{\rho}\right\}$$

$$= z_{ref} - \frac{1}{g}\left\{\frac{p_T}{\rho_S} + \frac{(p_{ref} - p_T)}{\rho_D}\right\} \qquad (11.5)$$

$$= z_{ref} - \frac{1}{g}\left\{p_T\left(\frac{1}{\rho_S} - \frac{1}{\rho_D}\right) + \frac{p_{ref}}{\rho_D}\right\}$$

$$= z_{ref} - \frac{1}{\rho_D g}\left(p_T\frac{\Delta\rho}{\rho_S} + p_{ref}\right)$$

$$= z_{ref} - \frac{1}{\rho_D g}[(z_T - z_S)g\Delta\rho + p_{ref}] \quad .$$

This shows that z_S becomes more negative, i.e. the sea surface becomes "higher," as the thermocline becomes deeper.

Consider a sloping thermocline below a sloping sea surface, as shown in Fig. 11.22. Define a transformed vertical coordinate which measures the depth below the thermocline:

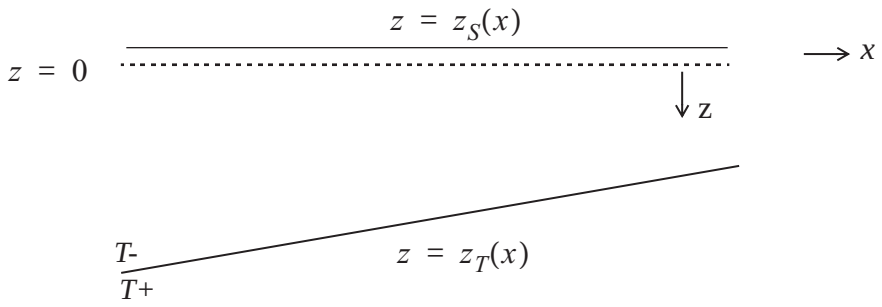

Figure 11.22:A sloping thermocline below a sloping sea surface.

$$z' \equiv z - z_T(x)\,. \tag{11.6}$$

The horizontal pressure gradient force can be written as

$$-\frac{1}{\rho}\left(\frac{dp}{dx}\right)_z = -\frac{1}{\rho}\left[\left(\frac{dp}{dx}\right)_{z'} - \frac{dp}{dz}\frac{dz_T}{dx}\right]. \tag{11.7}$$

This can be applied below and above the thermocline, as follows:

$$\begin{aligned} -\frac{1}{\rho_D}\left(\frac{dp}{dx}\right)_z\Bigg|_{z_{T+}} &= -\frac{1}{p_D}\left[\left(\frac{dp}{dx}\right)_{z'_{T+}} - \left(\frac{dp}{dz}\right)_{T+}\frac{dz_T}{dx}\right] \\ -\frac{1}{\rho_S}\left(\frac{dp}{dx}\right)_z\Bigg|_{z_{T-}} &= -\frac{1}{p_S}\left[\left(\frac{dp}{dx}\right)_{z'_{T-}} - \left(\frac{dp}{dz}\right)_{T-}\frac{dz_T}{dx}\right] \end{aligned} \tag{11.8}$$

But we assume that

$$\left.\frac{dp}{dx}\right|_{z'_{T+}} = \left.\frac{dp}{dx}\right|_{z'_{T-}}, \tag{11.9}$$

which means that the pressure is continuous across the thermocline, and

$$\left(\frac{dp}{dx}\right)_{z_{T+}} = 0 \tag{11.10}$$

which means that the is no pressure gradient below the thermocline. In addition, we use the hydrostatic equation, (11.3). Then we obtain

$$0 = -\frac{1}{\rho_D}\left[\left(\frac{dp}{dx}\right)_{z'_{T+}} - \rho_D g\frac{dz_T}{dx}\right]$$
$$-\frac{1}{\rho_S}\left(\frac{dp}{dx}\right)_z\Bigg|_{T-} = -\frac{1}{\rho_S}\left[\left(\frac{dp}{dx}\right)_{z'_{T-}} - \rho_S g\frac{dz_T}{dx}\right] \tag{11.11}$$

Substituting across gives

$$-\frac{1}{\rho_S}\left(\frac{dp}{dx}\right)_z\Bigg|_{T-} = -\frac{g}{\rho_S}(\rho_D - \rho_S)\frac{dz_T}{dx}. \tag{11.12}$$

We find that

$$-\frac{1}{\rho_S}\left(\frac{dp}{dx}\right)_z\Bigg|_{T-} = -g\frac{\Delta\rho}{\rho_S}\frac{dz_T}{dx} \tag{11.13}$$

For $\frac{dz_T}{dx} < 0$ (i.e., the thermocline slopes upward towards the east), we find that $-\frac{1}{\rho_S}\left(\frac{dp}{dx}\right)_z \geq 0$ (the water above the thermocline is pushed towards the east).

Assuming that ρ is independent of depth in the mixed layer, we can write

$$p(z) = \rho g(z - z_S) \text{ for } z < z_{T-} \quad . \tag{11.14}$$

Differentiation gives

$$\left(\frac{dp}{dx}\right)_z = g\left[\left(\frac{d\rho}{dx}\right)_z (z - z_S) - \rho_S\frac{dz_S}{dx}\right] \text{ for } z < z_{T-} \quad . \tag{11.15}$$

If the pressure gradient is vertically uniform in the mixed layer (which it will be if $\frac{d\rho_S}{dx} \cong 0$), then

$$\left(\frac{dp}{dx}\right)_z = -\rho_S g\frac{dz_S}{dx} = g\Delta\rho\frac{dz_T}{dx}, \tag{11.16}$$

and so by comparing (11.13) and (11.16) we find that

$$\frac{dz_S}{dx} = -\frac{\Delta\rho}{\rho_S}\frac{dz_T}{dx}. \tag{11.17}$$

This means that the sea surface slopes up where the thermocline slopes down. We can therefore use the slope of the sea surface to infer the slope of the thermocline. In addition, we can use the slope of the sea surface to infer the near-surface pressure-gradient force.

11.6 Summary